Temperature Cycling Effects Between Sn/Pb Solder and Thick Film Pd/Ag Conductor Metallization

Bi-Shiou Chiou, K. C. Liu, Jenq-Gong Duh, and P. Samy Palanisamy

Abstract—**Thermal cycling effects on solder joint between thick film mixed bonded conductor and Sn/Pb solder are investigated. Microstructural evolution of the interfacial morphology, elemental, and phase distribution are probed with the aid of electron microscopy and x-ray diffraction. Microstructural analysis reveals the formation of intermetallic compounds Pd_3Sn, Pd_2Sn, Pd_3Sn_2, PdSn, Pd_3Pb, Ag_5Sn, and Ag_3Sn, after thermal cycles from −55 to +125°C. A transverse crack is observed across the joint from the conductor/substrate interface to the conductor/solder interface, which results in the failure of the joint. The microstructural analysis and stress analysis reveal that the transverse crack is initiated by the microcracks at the glass penetrated region of the substrate and propagates under a tensile stress due to the solder shrinkage. An appropriate joint geometry and a materials system with good interface strength and with negligible thermal expansion mismatch are important in the enhancement of the life time for the solder joints in thick film microelectronics.**

I. Introduction

In THE thick film hybrid microelectronics industry, a wide range of metallized finishes can be applied on the ceramic substrate to form the circuit pattern for printed conductors. Interconnections between thick film conductors and discrete electronic devices are frequently made through a solder alloy screen printed or soldered into position. During the soldering operation and subsequent joint life, intermetallic compounds form and grow. The metallurgical reactions between the solder and conductor metallization can have a deleterious effect on the adhesion of the conductor to the underlying substrate, particularly when the assemblies are subjected to thermal aging and temperature cycling [1]–[6].

This paper reports on the second phase of an investigation undertaken to establish and to minimize potential reliability problems arising from the use of Pd/Ag in a hybrid manufacturing process. The first phase, reported in a previous paper [1], described the effect of intermetallic formation on the fracture of Sn/Pb solder and Pd/Ag conductor interfaces. The present paper deals with the temperature cycling effects between Sn/Pb solder and Pd/Ag conductor metallizations. The material systems in this study are 63/37 Sn/Pb solder™ and a commercial Pd/Ag conductor. The major constituents of the conductor detected by Atomic Emission Spectroscopy (AES, Shimadzu, Japan) are listed in Table I [1].

Manuscript received March 25, 1990; revised October 30, 1990. The work of B.-S. Chiou was supported by the National Science Council, Taiwan, under Contract NSC79-0404-E009-53.

B.-S. Chiou is with the Institute of Electronics, National Chiao Tung University, Hsinchu, Taiwan.

K. C. Liu and J.-G. Duh are with the Department of Materials Science and Engineering, National Tsing Hua University, Hsinchu, Taiwan.

P. S. Palanisamy is with Delco Electronics, General Motor Corporation, Kokomo, IN.

IEEE Log Number 9042165.

™Multicore Soldering Technology Ltd.

TABLE I
AES Results on Major Constituents of the Pd/Ag Conductor

Pd	Ag	Pb	Bi	Cu	Pd:Ag
		(Relative Concentration)*			
1036.4	8963.6	177.2	1242.4	6.67	1:8.65

*Normalized to Pd + Ag = 10 000

II. Experimental Procedure

The conductor paste was printed on the 96% Al_2O_3 substrate™ through a 325 mesh stainless steel screen with a pattern described in the previous work [1]. Samples were dried at 150°C for 15 min and then air fired in a belt furnace. The total firing cycle time was 32 min with 7 min of peak firing at 850°C. Wires were soldered to metallized substrate as reported previously [1]. Test samples were then subjected to thermal cycle test until samples failed, which indicated the loss of adhesion. Thermal cycle tests were performed with a 1-h cyclic period from −55 to 125°C between the freezing chamber and the oven. The specimen was first placed in the oven at 125°C for 25 min, taken out to the room temperature for 5 min, then put into the freezing chamber at −55°C for 25 min, and followed by a 5-min stay at room temperature before another thermal cycle. Microstructure and elemental distribution of the specimens were further investigated with a scanning electron microscope (SEM, S250 MK3, Cambridge, England) and an electron probe microanalyzer (EPMA, JCXA-733, JEOL, Japan).

III. Results and Discussion

The adhesion strength of the soldered pads drops to zero after 63 temperature cycles for most samples. The cross-sectional SEM micrographs and x-ray mapping of the as-soldered specimen and the failed sample (after 63 thermal cycles) are given in Figs. 1 and 2. Except for the transverse crack in the failed sample, the morphology after the thermal cycle is similar to that under the aging test [1], [6]. Some silver and palladium powders carried by the glass binder flow into the grain boundary of the substrate where sintering occurs. This enhances the mechanical interlock and thus increases the adhesion strength. Tin diffuses into the conductor, the bismuth rich phase penetrates into the substrate about 10 μm in depth, and the palladium layer is thicker than the silver one. The crack, propagated across the soldered thick film from the conductor/substrate interface up to the solder/conductor interface, results in the complete loss of

™AlSiMag 614, 3M Co., St. Paul, MN.

0048-6411/91/0300-0233$01.00 ©1991 IEEE

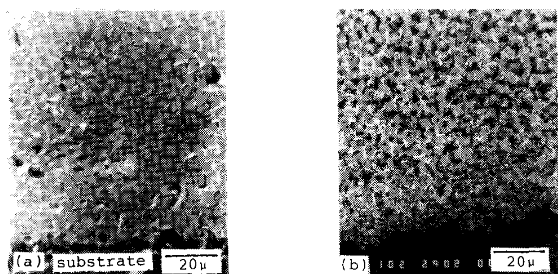

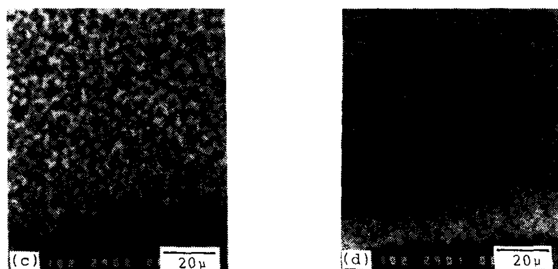

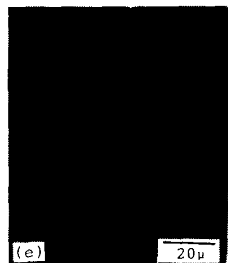

Fig. 1. Cross-sectional view of the as-soldered sample. (a) SEI picture. (b) Sn x-ray mapping. (c) Pb x-ray mapping. (d) Ag x-ray mapping. (e) Pd x-ray mapping.

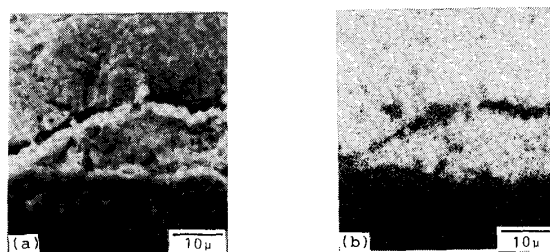

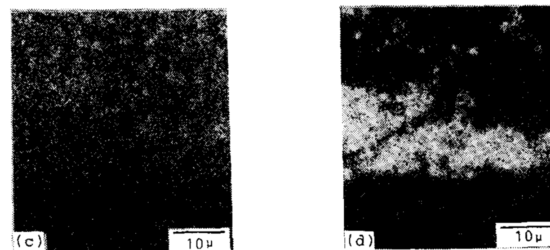

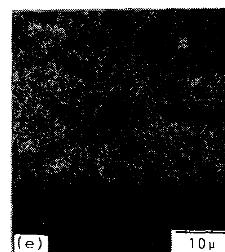

Fig. 2. Cross-sectional view of the sample after 63 thermal cycles. (a) SEI picture. (b) Sn x-ray mapping. (c) Pb x-ray mapping. (d) Ag x-ray mapping. (e) Pd x-ray mapping.

adhesion strength of the thermally cycled specimens. The x-ray diffraction pattern of the fracture surface reveals the coexistence of compounds Ag_5Sn, Ag_3Sn, Pd_3Sn, Pd_2Sn, Pd_3Sn_2, PdSn, and Pd_3Pb as shown in Fig. 3.

The intermetallic compounds form around the solder joint with Pd/Ag thick film conductor as the base metal after thermal cycling. Conductor swelling caused by tin diffusion into the conductor film, and volume change caused by the intermetallic formation, decease the strength of the soldered joint [1], [6].

The phases at the fracture surface are as complicated as those in the aging test. Pd_3Pb, a face-centered cubic structure with lattice constant about 4.204 Å, is the phase located at the interface near the solder. The crack propagates through Pd_3Pb to the solder/conductor interface [6].

A typical fracture surface of the substrate side, as shown in Fig. 4, is divided into two distinct regions including the substrate exposed region and the conductor region. At the conductor region, the surface morphology is almost the same as the fracture surface of the aging test specimen at the solder/conductor interface. At the substrate exposed region, there exists the reacted alumina, similar to the fractured structure in the aging test at the conductor/substrate interface [1]. However, in some areas, grains of alumina substrate can be observed as shown in Fig. 5(a), along with microcracks at the grain boundary. Cracks exist at both the reacted alumina region and the interfaces between reacted and unreacted grains, as indicated in Fig. 5(b)-(d). The bismuth rich phase segregates at the alumina grain boundary. During the thermal cycles, it is argued that the thermal expansion coefficient mismatch between the alumina grain and the bismuth rich produces the cracks. The bismuth penetrated region in thick film conductor fails to bear the cyclic thermal shock between -55 and 125°C.

The difference of the thermal expansion coefficients is always attributed to the joint failure under thermal cycling. To simulate the performance of the solder and alumina under the temperature ramping part of the thermal cycle, a thermal dilatometer (DL)™ was used to measure the extent of the solder and alumina expansion with a fast temperature ramping rate. A 12.85-mm solder bar was tested under furnace temperature ramp rates of 4 and 15°C/s, from room temperature to 120°C. A 13.55-mm alumina slice was tested with the same rates, up to 130°C.

The solder, with a larger thermal expansion coefficient and thermal conductivity as listed in Table II, should have a faster temperature rise and greater thermal strain. Fig. 6(a) and (b) indicates the typical curves for temperature rise and expansion versus time. For the furnace temperature ramp rate at 4°C/s, after a finite delay time, the solder exhibits an initial strain rate of 47.54×10^{-6} $\mu m/\mu m \cdot s$ and a temperature rising rate of

™DL-1500, ULVAC, Tokyo, Japan.

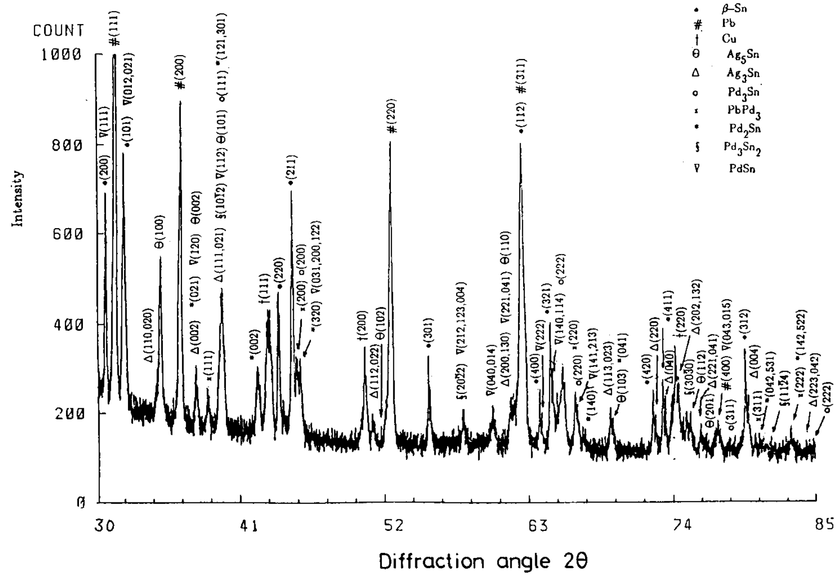

Fig. 3. X-ray diffraction pattern of the fracture surface for samples after 63 temperature cycles.

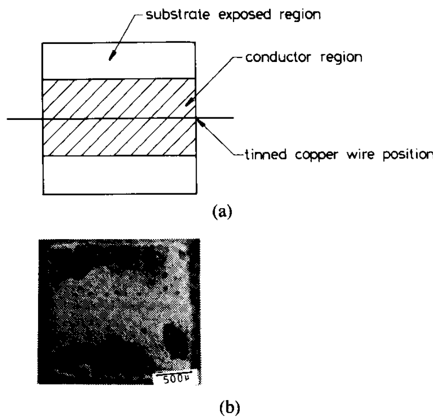

Fig. 4. Top view of a typical fracture surface in the substrate side.

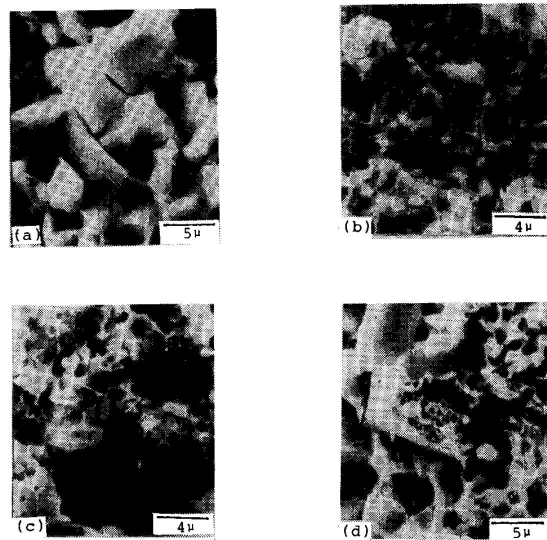

Fig. 5. SEM micrographs at the substrate exposed region for the failed joint with 63 thermal cycles. (a) Microcracks between exposed alumina grain. (b) Cracks exist at the reacted alumina substrate. (c) Cracks between the alumina grain and reacted alumina substrate. (d) Cracks between the alumina grain and the reacted alumina substrate with the Bi-rich phase.

8.11°C/s. For alumina, the initial strain and temperature rising rates are 11.04×10^{-6} μm/μm · s and 4.44°C/s, respectively. For the temperature ramp rate at 15°C/s, the alumina strain rate become 23.98×10^{-6} μm/μm · s, while it is 169.3×10^{6} μm/μm · s for the solder. This implies that if the environmental temperature changes rapidly, as in the ramping part and the falling part during the thermal cycle, both the solder and alumina expand and shrink with different rates. The faster the environmental temperature changes, the more enhanced the strain rate difference is.

The joint geometry is another factor which affects the joint's failure. The difference of the thermal expansion coefficients introduces the stress, and the joint geometry defines where the stress is created during thermal cycling. The inclined surface of the solder fillet at both sides of the test pad casts a stress with an elevation angle, as shown in Fig. 7 , which is resolved into tensile and shear components. Near the copper wire, the stress

TABLE II
THERMAL EXPANSION COEFFICIENTS OF SELECTED MATERIALS

	Thermal expansion coefficient (μ/°C)
solder(63/37)	24.7
Al_2O_3	8.8
Cu	16.6
Pd	11.8
Ag	18.9

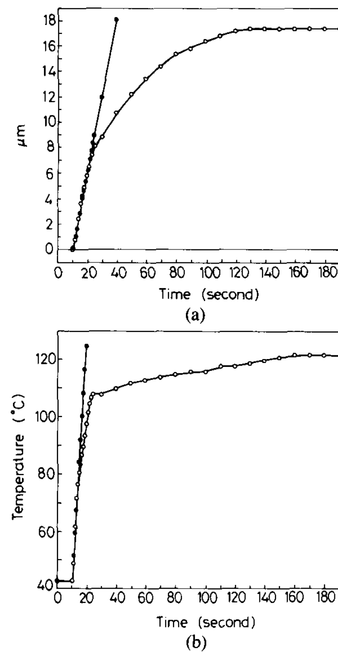

Fig. 6. (a) Solder expansion at 4°C/s furnace temperature ramp rate in the thermal dilatometer. The initial expansion rate is indicated. (b) Solder temperature rise at 4°C/s furnace temperature ramp rate in thermal dilatometer. The initial temperature rise rate is indicated.

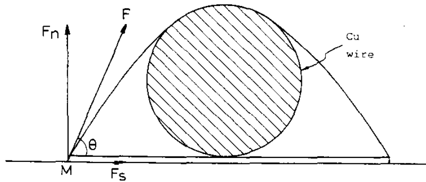

Fig. 7. A schematic diagram shows the solder shrinkage force, F, applied on the conductor/substrate interface. The force F is resolved into the tensile component, F_n, and shear component, F_s.

field becomes simply shear due to the thermal expansion coefficient misfit between the copper wire and the substrate.

The top view of test pads shows two distinct regions corresponding to various stress fields. The characteristics of the two regions, the conductor/substrate interface and the conductor/solder interface, have been discussed previously [1], [6]. The mechanism of the transverse crack initiation and propagation can then be proposed. The transverse crack initiates at the conductor/substrate interface where microcracks exist, and the tensile stress drives the crack to propagate along the conductor/substrate interface. When the tensile stress is reduced, the overall stress field is dominated by the shear stress, and the crack propagates up to the solder/conductor interface, as illustrated in Fig. 8.

Occasionally, the crack propagates down to the alumina substrate, as shown in Fig. 9. The possibility is about 10% of the total joints, and this is just a localized phenomenon. The occurrence of this condition lies on the accidental tangle of the transverse crack and the downward microcracks at the alumina grain boundary.

The strength of the interface, joint geometry, and the materi-

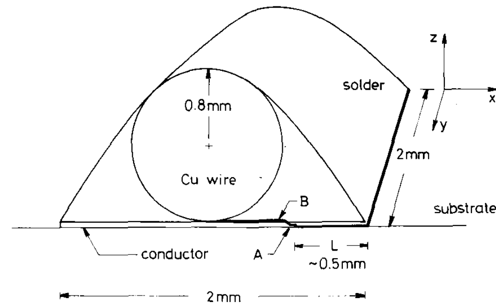

Fig. 8. A schematic diagram illustrates the crack configuration and the shear stress effect on the solder/conductor interface. Point A indicates the breaking point of the crack propagation at the conductor/substrate interface. Point B indicates the beginning of the crack propagation at the solder/conductor interface.

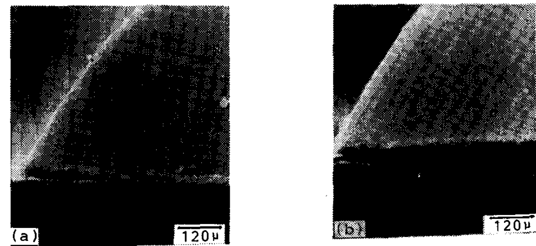

Fig. 9. Transverse crack results in joint failure. (a) Crack propagates along conductor/substrate interface, then up to solder/conductor interface. (b) Crack propagates down to the substrate.

als system determine the location where the failure takes place. For thick film conductor, the interface strength is not strong enough to bear the cyclic stress, and the joint failure occurs before the solder fatigue is reached. In the practical application, approaches to design an appropriate joint geometry, to improve the interface strength, and to select the materials system with negligible thermal expansion coefficient mismatch will be crucial to increase the life time of the solder joints in thick film microelectronic packages.

IV. Summary and Conclusions

1) Temperature cycling effects between thick film mixed conductor and Sn/Pb solder are evaluated. Microstructural analysis of the soldered conductor/substrate assembly reveals the existence of mechanical interlocking between conductor and substrate. X-ray diffraction results suggest the formation of intermetallic compounds Ag_5Sn, Ag_3Sn, Pd_3Sn, Pd_2Sn, Pd_3Sn_2, PdSn, and Pd_3Pb during thermal cycling.
2) Conductor swelling caused by tin diffusion into the conductor, and volume change caused by the intermetallic formation, degrade the strength of the solder joint.
3) The thick film soldered joint fails to sustain a stress with the tensile component under thermal cycles. This is related to the cracks existing at the glass penetrated region of the conductor/substrate interface, where the transverse crack resulting in the joint failure is initiated.
4) An appropriate joint geometry and a materials system with good interface strength and with negligible thermal expansion mismatch are crucial to increase the reliability of solder joints in thick film microelectronics.

Acknowledgment

This paper was initiated at Delco Electronics, General Motor Corporation, Kokomo, IN, during the on-leave period of one of the authors, B.-S. Chiou. She appreciates the support and friendship from the Delco Group.

References

[1] B. S. Chiou, K. C. Liu, J. G. Duh, and P. Palanisamy, "Intermetallic formation on the fracture of Sn/Pd solder and Pd/Ag conductor interfaces," *IEEE Trans. Compo., Hybrids, Manuf. Technol.*, vol. 13, pp. 267–274, 1990.

[2] R. H. Short and G. P. Evans, "Soldering as a forethought," *Assembly Eng.*, vol. 3, pp. 44–47, 1988.

[3] R. Chadwick, "The influence of surface alloying on strength of soft soldered joints," *J. Inst. Metals*, vol. 62, pp. 277–295, 1938.

[4] G. C. Smith and C. Lea, "Wetting and spreading of liquid metals: The role of surface composition," *Surface Interface Anal.* vol. 9, pp. 145–150, 1986.

[5] J. A. DeVore, "Solderability," *J. Metals*, pp. 51–53, July 1984.

[6] K. C. Liu, "Solder-conductor interaction and dielectric-substrate interfacial phenomenon in hybrid circuit," Master's thesis, National Tsing Hua University, Hsinchu, Taiwan, May 1989.

[7] H. A. H. Steen and G. Becker, "The effect of impurity elements on the soldering properties of eutectic and near-eutectic tin-lead solder," *Brazing Soldering*, vol. 11, pp. 4–11, 1986.

[8] W. D. Kingery, H. K. Bowen, and D. R. Uhlmann, *Introduction to Ceramics*, 2nd ed. New York: Wiley, 1976, p. 595.

[9] *CRC Handbook of Chemistry and Physics*, R. C. Weast, Ed. CRC, 1980.